
Molecular Imaging of Neuroendocrine Prostate Cancer by Targeting Delta-Like Ligand 3

Joshua A. Korsen^{1,2}, Teja M. Kalidindi¹, Samantha Khitrov¹, Zachary V. Samuels¹, Goutam Chakraborty^{3,4}, Julia A. Gutierrez¹, John T. Poirier⁵, Charles M. Rudin^{2,3}, Yu Chen^{3,6}, Michael J. Morris³, Nagavarakishore Pillarsetty¹, and Jason S. Lewis^{1,2}

¹Department of Radiology, Memorial Sloan Kettering Cancer Center, New York, New York; ²Department of Pharmacology, Weill Cornell Medicine, New York, New York; ³Department of Medicine, Memorial Sloan Kettering Cancer Center, New York, New York; ⁴Department of Urology, Icahn School of Medicine at Mount Sinai, New York, New York; ⁵Perlmutter Cancer Center, New York University Langone Health, New York, New York; and ⁶Human Oncology and Pathogenesis Program, Memorial Sloan Kettering Cancer Center, New York, New York

Treatment-induced neuroendocrine prostate cancer (NEPC) is a lethal subtype of castration-resistant prostate cancer. Using the ⁸⁹Zr-labeled delta-like ligand 3 (DLL3) targeting antibody SC16 (⁸⁹Zr-desferrioxamine [DFO]-SC16), we have developed a PET agent to noninvasively identify the presence of DLL3-positive NEPC lesions. **Methods:** Quantitative polymerase chain reaction and immunohistochemistry were used to compare relative levels of androgen receptor (AR)-regulated markers and the NEPC marker DLL3 in a panel of prostate cancer cell lines. PET imaging with ⁸⁹Zr-DFO-SC16, ⁶⁸Ga-PSMA-11, and ⁶⁸Ga-DOTATATE was performed on H660 NEPC-xenografted male nude mice. ⁸⁹Zr-DFO-SC16 uptake was corroborated by biodistribution studies. **Results:** In vitro studies demonstrated that H660 NEPC cells are positive for DLL3 and negative for AR, prostate-specific antigen, and prostate-specific membrane antigen (PSMA) at both the transcriptional and the translational levels. PET imaging and biodistribution studies confirmed that ⁸⁹Zr-DFO-SC16 uptake is restricted to H660 xenografts, with background uptake in non-NEPC lesions (both AR-dependent and AR-independent). Conversely, H660 xenografts cannot be detected with imaging agents targeting PSMA (⁶⁸Ga-PSMA-11) or somatostatin receptor subtype 2 (⁶⁸Ga-DOTATATE). **Conclusion:** These studies demonstrated that H660 NEPC cells selectively express DLL3 on their cell surface and can be noninvasively identified with ⁸⁹Zr-DFO-SC16.

Key Words: neuroendocrine prostate cancer; immuno-PET; molecular imaging; DLL3

J Nucl Med 2022; 63:1401–1407
DOI: 10.2967/jnumed.121.263221

Androgen receptor (AR) signaling is a critical driver of prostate cancer (PC). Androgen deprivation therapy (ADT) is used in the setting of high-risk, recurrent, or metastatic PC. Although ADT can initially be highly effective, resistance develops in most patients, leading to metastatic castration-resistant PC (mCRPC) and ultimately death. Treatment resistance to ADT in mCRPC arises from multiple mechanisms including AR amplification, AR bypass, and complete

AR independence (1). The introduction of more potent AR signaling inhibitors (e.g., abiraterone and enzalutamide) in mCRPC patients has led to an increasing incidence of lesions that may display AR loss or adapt to low androgen levels through activation of alternative pathways (2). AR-independent tumors can be aggressive and can demonstrate markedly elevated proliferation, an enhanced capacity for organ metastasis, and phenotypic heterogeneity with a variable admixture of adenocarcinoma and small cell neuroendocrine phenotypes (2). Treatment-induced neuroendocrine PC (NEPC) has been shown to arise from treatment-induced lineage plasticity and to lead to a highly aggressive and lethal subtype of PC (3). This reprogramming is linked to the reactivation of developmental transcriptional programs and the transcription factor SOX2, which promotes phenotypic plasticity and acquisition of a stemlike phenotype (4). NEPC displays genetic similarities to small cell lung cancer (SCLC), including frequent loss of the tumor suppressor genes *TP53* and *RBI* (5).

The lineage transcription factor achaete-scute complex homolog 1 (ASCL1) is overexpressed and promotes tumorigenesis in mouse models of SCLC (6). ASCL1 plays a key role in suppressing notch signaling activity through markedly upregulated expression of the inhibitory notch ligand delta-like ligand 3 (DLL3) (7). DLL3 expression in adult tissues is substantially lower and restricted to intracellular compartments such as the Golgi; in contrast, in SCLC tumor cells DLL3 is aberrantly expressed on the cell surface (7). In PC, DLL3 has been shown to be similarly dysregulated in most NEPC samples (76.6%), with minimal to no expression in mCRPC (12.5%), localized PC (0.5%), and normal, unaffected prostate tissue (0%) (8). With no detectable expression of cell surface DLL3 in nonmalignant cells and preferential expression in NEPC lesions, DLL3 may be a target for a biomarker-based method of tumor detection.

SC16 is a humanized monoclonal antibody that selectively binds to both human and murine DLL3 (9). Our previous work with SC16 demonstrated the successful synthesis of ⁸⁹Zr-radiolabeled SC16 and its use as a PET radiopharmaceutical for noninvasive detection of DLL3 expression in SCLC models (10). PET is a powerful diagnostic tool that can noninvasively visualize and molecularly characterize lesions and aid in optimizing therapy. It has proven to be a successful platform in PC detection and management of AR-dependent lesions. However, the 2018 National Cancer Institute Workshop on Lineage Plasticity and Androgen Receptor-Independent Prostate Cancer identified a “lack of imaging capabilities” as 1 of 2 major knowledge gaps in NEPC management (11). The PET probes thus far developed directly target AR (12) or prostate-specific membrane antigen (PSMA)

Received Oct. 3, 2021; revision accepted Jan. 12, 2022.
For correspondence or reprints, contact Nagavarakishore Pillarsetty (pillarsn@mskcc.org) or Jason S. Lewis (lewisj2@mskcc.org).
Published online Jan. 20, 2022.
COPYRIGHT © 2022 by the Society of Nuclear Medicine and Molecular Imaging.

(13) and may not detect NEPC lesions if they display AR loss or PSMA suppression (14). Therefore, it is imperative to have a non-PSMA-based imaging agent for NEPC detection. To our knowledge, ^{89}Zr -radiolabeled SC16 is the only imaging agent currently in development that has potential to differentiate NEPC from prostate adenocarcinoma by an increase in signal above background. This is advantageous over current PET imaging agents that target AR-dependent PC, as reduced expression of these surface antigens is possible and can increase susceptibility to high false-positives or inconclusive findings when signal approaches the noise floor. Because of the molecular similarities to SCLC and encouraging results from preclinical studies in SCLC models, we evaluated the performance of our ^{89}Zr -radiolabeled SC16 PET imaging agent in the detection of DLL3-expressing NEPC tumors in preclinical mouse models.

MATERIALS AND METHODS

The supplemental materials (available at <http://jnm.snmjournals.org>) provide information on cell lines, quantitative real-time polymerase chain reaction, antibody functionalization and radiolabeling (15), in vitro binding assays (16), immunohistochemistry, and generation of subcutaneous xenograft models.

Animals and Tumor Models

All animal experiments were approved by the Institutional Animal Care and Use Committee and Research Animal Resource Center at Memorial Sloan Kettering Cancer Center.

Biodistribution Studies

Biodistribution studies were performed by killing mice bearing subcutaneous H660 or DU145 tumors at chosen time points to evaluate uptake of the radiotracers. To evaluate nonspecific uptake in the DLL3-positive tumor, mice bearing subcutaneous H660 xenografts were injected with isotype-matched IgG ^{89}Zr -desferrioxamine (DFO)-IgG. The supplemental materials provide further details.

PET Imaging

PET imaging of subcutaneous PC cell line xenograft mouse models was performed on an Inveon small-animal PET/CT instrument (Siemens). The supplemental materials provide further details.

Statistical Analysis

Data are expressed as mean \pm SEM. Data for the in vitro cell binding assay were analyzed by unpaired, 2-tailed *t* testing using Prism software (version 8; GraphPad), with the threshold for statistical significance set at a *P* value of less than 0.05. To evaluate the blocking study in the subcutaneous xenografts, a 2-way ANOVA test using Prism software was performed, with the threshold for statistical significance set at a *P* value of less than 0.05. A correction for multiple comparisons was performed using the Holm-Sidak method to determine statistical significance ($\alpha = 0.05$).

RESULTS

Evaluation of DLL3 Expression in NEPC

We evaluated messenger RNA and protein expression of AR and SOX2 transcription

factors and their downstream targets that have been shown to differentiate adenocarcinoma or neuroendocrine phenotype, respectively, in established PC cell lines using quantitative real-time polymerase chain reaction and immunohistochemistry. For prostate adenocarcinoma genes, we evaluated *FOLH1* (gene encoding for PSMA) and *KLK3* (gene encoding for prostate-specific antigen); for neuroendocrine-regulated genes, we examined *ASCL1* and *DLL3*. The panel of PC cell lines included LNCaP (hormone-sensitive prostate adenocarcinoma, AR-positive/neuroendocrine-negative), DU145 (androgen-independent PC, AR-negative/neuroendocrine-negative), PC3 (androgen-independent PC, AR-negative/neuroendocrine-negative), and H660 (NEPC, AR-negative/neuroendocrine-positive). H660 expressed the highest of *SOX2*, which encodes a transcription factor that promotes lineage plasticity, facilitates histologic transformation, and has been associated with resistance to AR-targeted therapies (5,17). PC3, LNCaP, and DU145 all demonstrated significantly lower levels of *DLL3*. H660 cells showed *ASCL1* expression, encoding a key transcription regulator of notch signaling proteins, including *DLL3* (Fig. 1A). At the protein level, using immunohistochemistry, we could detect *DLL3* expression only in the H660 line, not in the other PC lines (Fig. 1B). Verification of the NEPC lineage of H660 was confirmed by the presence of the clinically validated neuroendocrine marker synaptophysin (SYP), which was absent in all LNCaP, PC3, and DU145 cell lines (Fig. 1B). When transcript levels of *AR*, *KLK3*, and *FOLH1* were evaluated, only LNCaP cells showed

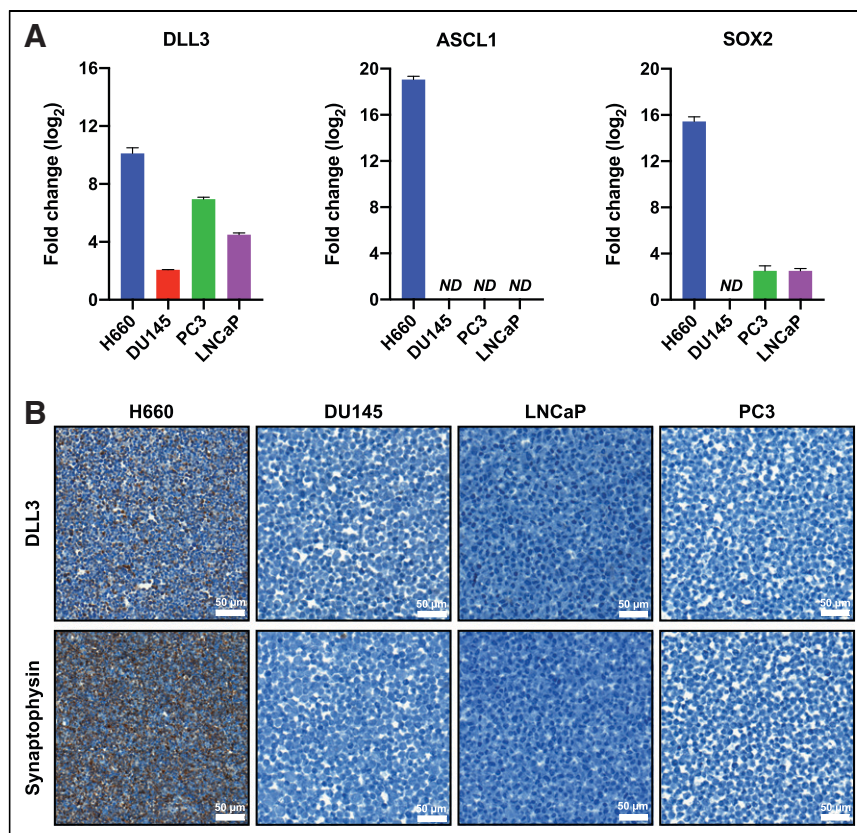


FIGURE 1. DLL3 is uniquely expressed in H660 cells at transcriptional and translational level. (A) Real-time polymerase chain reaction shows expression patterns of *DLL3*, *ASCL1*, and *SOX2* genes in H660, DU145, PC3, and LNCaP cells compared with A549-negative control (not shown). (B) Representative immunohistochemistry images of H660 (DLL3-positive/SYP-positive), DU145 (DLL3-negative/SYP-negative), LNCaP (DLL3-negative/SYP-negative), and PC3 (DLL3-negative/SYP-negative) tumor cell sections for DLL3 and SYP. ND = not detected.

expression, whereas H660, PC3, and DU145 had minimal detectable transcripts (Supplemental Fig. 1A). Immunohistochemistry provided similar results at the translational level, demonstrating intense staining of AR and PSMA in LNCaP cells, with no detectable expression seen in H660, PC3, or DU145 (Supplemental Fig. 1B).

We then analyzed the PC transcriptomic atlas dataset (18), an extensive transcriptome databank comprising 1,321 clinical specimens from 38 PC cohorts. We observed higher expression of *DLL3* in mCRPC than in primary PC ($P < 0.001$ mCRPC vs. primary; Supplemental Fig. 2A). Moreover, in the cohort of Ross-Adams et al. (19) (259 men with PC in Cambridge discovery cohort and Stockholm validation cohort), we found that high *DLL3* expression was associated with shorter biochemical recurrence-free survival (Supplemental Fig. 2B). Together, these data indicate that *DLL3* messenger RNA expression may be associated with a poor prognosis for PC patients. This hypothesis will require further testing in a larger cohort to confirm the prognostic significance of *DLL3* messenger RNA expression in PC.

We next compared the expression levels of *DLL3* in H660 and H82 tumor cells. H82 was derived from the pleural fluid of a patient with SCLC and H660 derived from the lymph node of an NEPC patient. Both cell lines displayed a neuroendocrine phenotype and aberrant *DLL3* trafficking to the cell surface. Despite low expression of *DLL3* on H82 cells, PET imaging successfully delineated H82 tumor in mouse models (10). Immunohistochemistry demonstrated an even lower abundance of *DLL3* expression in the H660 tumor cells than in the H82 tumor cells (Supplemental Fig. 3). However, we still envision that *DLL3* PET imaging would be feasible because of the absence of *DLL3* expression on the cell surface of nonmalignant cells.

⁸⁹Zr-DFO-SC16 Characterization and Its Detection of Cell Surface *DLL3* Expression

The *DLL3*-targeting SC16 antibody was functionalized through non-site-specific conjugation to the free lysine moieties available on the monoclonal antibody with the siderophore-derived DFO chelator (Supplemental Fig. 4). Matrix-assisted laser desorption/ionization time-of-flight mass spectrometry revealed that the ratio of chelator to monoclonal antibody was 0.44, which implies that,

on average, half of the antibody molecules were functionalized with DFO covalently (Supplemental Fig. 5).

Radiolabeling of the DFO-SC16 conjugate provided ⁸⁹Zr-DFO-SC16 in high radiochemical yield (>99%) (Supplemental Fig. 6A) and high specific activity (370 MBq/mg). The radioimmunoconjugate demonstrated at least 92% stability when incubated in human serum at 37°C for 5 d (Supplemental Fig. 6B). The target-binding fraction of the radioimmunoconjugate—the fraction of the antibody that retains its binding to its target after modification—was more than 90% for ⁸⁹Zr-DFO-SC16 toward *DLL3* (Fig. 2A). ⁸⁹Zr-DFO-SC16 binding to *DLL3* could be blocked in the presence of a 5,000-fold excess of unlabeled SC16. In vitro cell binding assays revealed ⁸⁹Zr-DFO-SC16 to be bound to *DLL3* expressed on the cell surface of H660 cells, with no binding observed in the *DLL3*-negative cell lines LNCaP, DU145, or PC3 (Fig. 2B). Binding of ⁸⁹Zr-DFO-SC16 to H660 cells could be blocked in the presence of a 1,000-fold excess of unlabeled SC16. A saturation binding assay with H660 cells revealed a dissociation constant of less than 1 nM and a maximum specific binding of 86.3 fM/10⁶ cells for ⁸⁹Zr-DFO-SC16 (Supplemental Fig. 6C). These studies demonstrated that the immunoreactivity of SC16 is retained after DFO conjugation and radiolabeling with ⁸⁹Zr.

PET Imaging and Biodistribution of *DLL3* Expression with ⁸⁹Zr-DFO-SC16 in Subcutaneous Xenograft Models

PET imaging with ⁸⁹Zr-DFO-SC16 was performed on male nude mice bearing H660 (*DLL3*-positive, AR-negative/neuroendocrine-positive) or DU145 (*DLL3*-negative, AR-negative/neuroendocrine-negative) subcutaneous xenografts. PET imaging with ⁸⁹Zr-DFO-SC16 showed clear delineation of H660 tumor xenografts 120 h after administration of the radioimmunoconjugate (Fig. 3A). Increasing uptake in the H660-bearing mice could be observed in the tumors from the time of injection to 120 h after injection. As expected, because of lack of *DLL3* expression, minimal uptake of ⁸⁹Zr-DFO-SC16 was observed in DU145-bearing mice, with tumor uptake remaining constant over the 120-h imaging time course (Fig. 3B). Low and nonspecific uptake was observed in H660 tumor xenografts 120 h after injection of isotype-matched IgG (⁸⁹Zr-DFO-IgG) (Supplemental Figs. 7A–7C).

Biodistribution data at 24, 72, and 120 h after intravenous administration confirmed a progressive increase in H660 tumor uptake over time, reaching 17.50 ± 3.19 percentage injected dose per gram (%ID/g) at 120 h (Fig. 4A; Supplemental Fig. 8). As expected, a concurrent decrease in blood-pool activity was observed (24 h, 6.60 ± 0.90 %ID/g; 72 h, 3.16 ± 1.37 %ID/g; 120 h, 3.07 ± 0.45 %ID/g) as the tumor activity increased over time. Because of heterogeneous uptake of the radioimmunoconjugate between the H660 tumors, 2 independent cohorts of 3 mice each were evaluated at 120 h. Linear regression analysis displayed a positive correlation between time after intravenous administration and %ID/g in H660 tumors across both independent cohorts, with tumor uptake increasing over time ($P = 0.00971$; Supplemental Fig. 9). Uptake of the radioimmunoconjugate could be blocked by coinjection of a 50-fold excess of unlabeled SC16 antibody, confirming the specificity of the radioimmunoconjugate for the H660 tumor (Fig. 4A; Supplemental Fig. 10). At 120 h after injection,

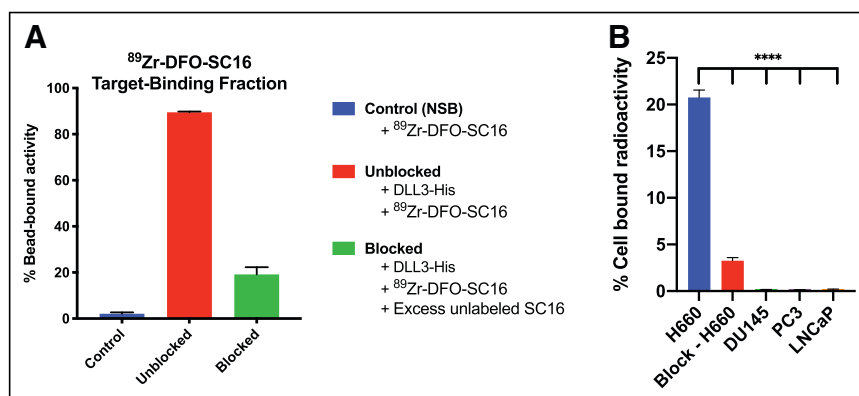


FIGURE 2. *DLL3* is expressed on cell surface of H660 tumor cells that can be targeted by ⁸⁹Zr-DFO-SC16. (A) ⁸⁹Zr-DFO-SC16 shows high and specific binding to Ni-NTA beads coated with His-tagged *DLL3*. Minimum nonspecific binding is observed (control). Specificity of binding to His-tagged *DLL3* was shown in presence of 5,000-fold excess of unlabeled SC16. (B) In vitro cell binding data on ⁸⁹Zr-DFO-SC16 binding to H660 cells confirms *DLL3* expression on cell surface that can be targeted using our anti-*DLL3* monoclonal antibody SC16. Minimal binding of ⁸⁹Zr-DFO-SC16 is observed to *DLL3*-negative DU145, PC3, and LNCaP cells. Specificity of binding to H660 cells was shown in presence of 1,000-fold excess of unlabeled SC16. **** $P < 0.0001$. NSB = nonspecific binding.

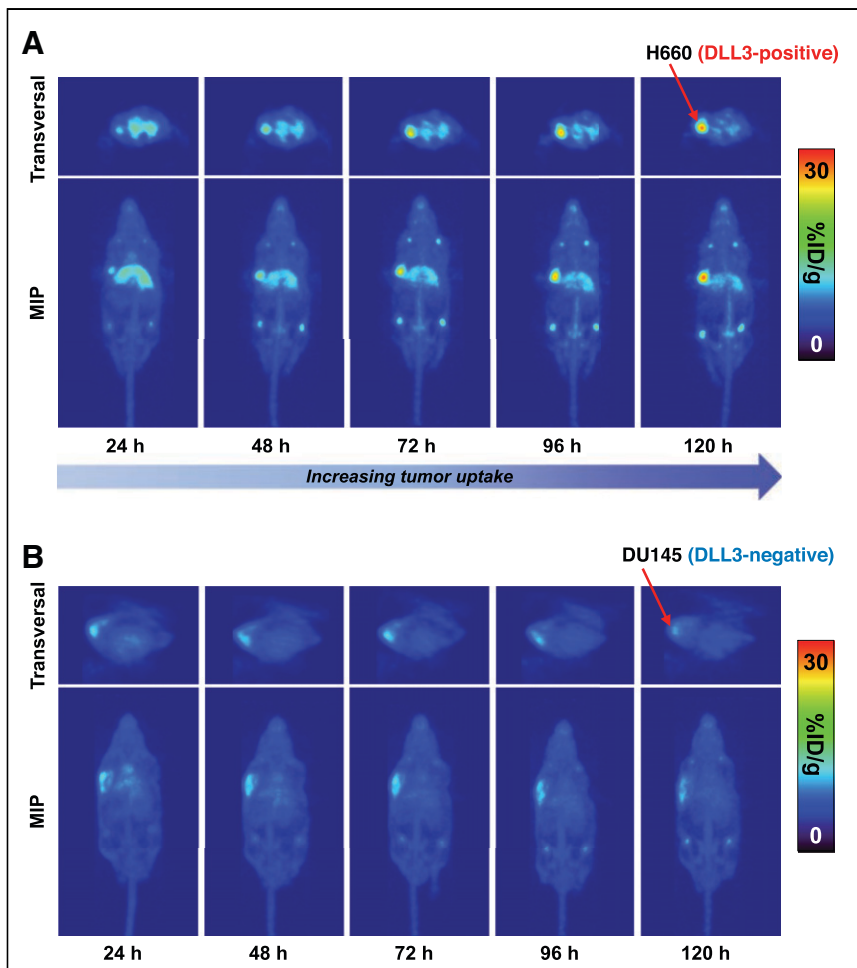


FIGURE 3. DLL3-expressing subcutaneous H660 tumors could be imaged with ^{89}Zr -DFO-SC16 in vivo. (A) PET images of ^{89}Zr -DFO-SC16 in athymic nude male mouse bearing subcutaneous H660 tumor xenografted on left shoulder. PET imaging was performed at 24-h intervals up to 120 h after injection of ^{89}Zr -DFO-SC16. (B) PET images of ^{89}Zr -DFO-SC16 in athymic nude male mouse bearing subcutaneous DU145 tumor xenografted on left shoulder. PET imaging was performed at 24-h intervals up to 120 h after injection of ^{89}Zr -DFO-SC16. Images represent maximum-intensity projection and transverse planar images at designated time points after injection of radiotracer. MIP = maximum-intensity projection.

high tumor-to-background contrast ratios were observed (Fig. 4B), with a tumor-to-muscle ratio of 33.91 ± 5.73 . In contrast, ^{89}Zr -DFO-SC16 uptake in the DU145 (DLL3-negative) tumors was low and nonspecific, at 5.47 ± 0.25 %ID/g 120 h after intravenous administration, consistent with an in vivo enhanced permeability and retention effect (Fig. 4C; Supplemental Fig. 11). Comparing tumor uptake at each time point in the H660 and DU145 tumors demonstrated the specificity and selectivity of ^{89}Zr -DFO-SC16 for DLL3 (Supplemental Fig. 12A). Mean uptake in H660 tumors increased over time and was statistically significant when compared with mean uptake in DU145 tumors at 72 and 120 h after injection. Tumor-to-muscle ratios also increased over time in the H660 tumors and were statistically significant at 72 and 120 h after injection when compared with DU145 tumors, in which this ratio remained relatively constant at all time points (Supplemental Fig. 12B). Considering potential clinical implications, taken together these data suggest that patients could be effectively imaged in a wide time window (72–120 h). Immunohistochemistry on resected H660

subcutaneous xenografts confirmed retained expression of DLL3 and SYP, which were absent in resected DU145 subcutaneous xenografts (Fig. 4D; Supplemental Fig. 13 shows SYP immunohistochemistry and corresponding hematoxylin- and eosin-stained slides).

NEPC Is Detectable Only by DLL3 Imaging, Not by PSMA or Somatostatin Imaging

To demonstrate the dichotomy between AR-positive prostate adenocarcinoma and AR-negative NEPC, male nude mice were subcutaneously xenografted with PSMA-positive/DLL3-negative LNCaP tumors and PSMA-negative/DLL3-positive H660 tumors on opposite flanks and imaged by DLL3- and PSMA-based PET. The dually tumor-bearing mice were imaged 1 h after administration of ^{68}Ga -PSMA-11, a PSMA-targeted PET agent. The radiotracer accumulated exclusively in the LNCaP tumor and could be successfully imaged with high contrast (Fig. 5). The NEPC model H660 does not express AR or PSMA, and H660 tumors could not be detected through PSMA-based imaging. Two days later, the same cohort of mice was administered ^{89}Zr -DFO-SC16 and imaged 5 d after administration. The radiotracer selectively bound to the H660 tumor but not to LNCaP and finally allowed for site-specific identification of the NEPC lesion.

Somatostatin receptor (SSTR) imaging has been widely used as a method to detect the presence of gastroenteropancreatic neuroendocrine neoplasms, including the Food and Drug Administration-approved agent ^{68}Ga -DOTATATE. ^{68}Ga -DOTATATE is a peptide-based PET imaging agent that demonstrates high affinity for the SSTR subtype 2 (SSTR2) and has been tested in NEPC patients with inconclusive results (20). As a comparator, we sought to image tumor-bearing mice by ^{68}Ga -DOTATATE. We first analyzed *SSTR2* messenger RNA expression in H660 and LNCaP cells. We could not detect significantly upregulated *SSTR2* expression in H660 cells relative to LNCaP cells (Supplemental Fig. 14A). Shifting to in vivo analysis, we conducted an imaging study with ^{68}Ga -DOTATATE on H660-bearing male nude mice. No accumulation of the radiotracer was observed in the tumor 1 h after administration, demonstrating an inability to detect this NEPC tumor through SSTR imaging (Supplemental Fig. 14B).

DISCUSSION

NEPC is a lethal disease, and detecting the presence of NEPC lesions noninvasively remains challenging. One of the barriers to understanding the biology of mCRPC is the inaccessibility of the tissue and consequent undersampling of disease heterogeneity. Biopsies (the gold standard in terms of phenotypic characterization with immunostaining) and genotypic characterization with next-generation sequencing techniques describe only a single lesion

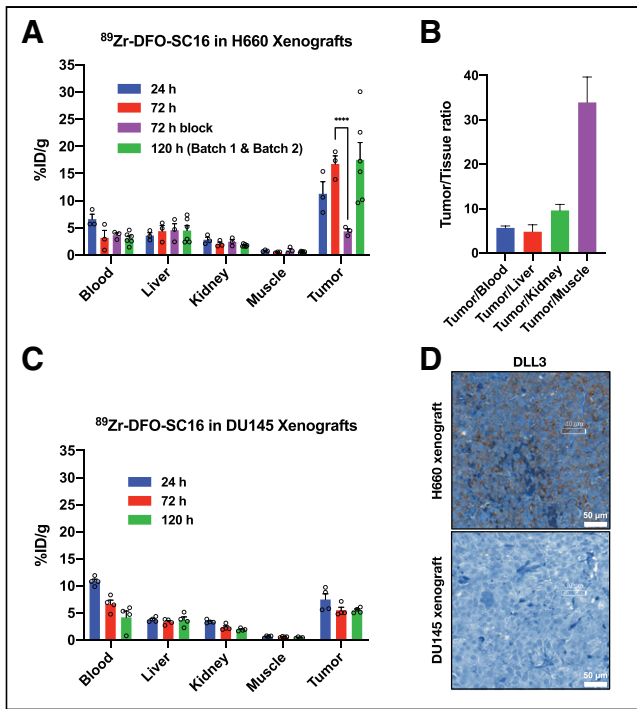


FIGURE 4. Biodistribution of ⁸⁹Zr-DFO-SC16 in subcutaneous xenograft model of NEPC. (A) Select organ biodistribution data at 24, 72, and 120 h after intravenous injection of ⁸⁹Zr-DFO-SC16 in athymic nude mice bearing subcutaneous H660 tumors. Bars at 24 and 72 h represent data obtained from batch 1 ($n = 3$). Bars at 120 h represent data obtained from batches 1 and 2 ($n = 6$). Supplemental materials provide details on the 2 different cohorts used in biodistribution study. H660 tumor uptake could be blocked at 72 h after injection of ⁸⁹Zr-DFO-SC16 with 50-fold excess of unlabeled SC16 antibody. (B) Tumor-to-background contrast ratios from uptake of ⁸⁹Zr-DFO-SC16 in H660 xenograft-bearing mice. (C) Select organ biodistribution at 24, 72, and 120 h after injection of ⁸⁹Zr-DFO-SC16 in athymic nude mice bearing subcutaneous DU145 tumors. (D) Representative immunohistochemistry images of H660 and DU145 subcutaneous tumor xenografts for DLL3. **** $P < 0.0001$.

rather than the full diversity of the disease. Furthermore, bone biopsies are difficult because tumors are frequently embedded deep within the densely sclerotic bone, a result of exuberant hydroxyapatite deposition from tumoral stimulation of osteoblasts. Circulating tumor cells and cell-free DNA can be used to characterize the biology of mCRPC and can reflect posttreatment changes in tumor burden but cannot localize the emergence of resistant disease on a lesional level. A noninvasive, whole-body method for detecting the emergence of NEPC will overcome these limitations of standard methods of tumor analysis, allow for identification and characterization of lesions in real time, and facilitate earlier intervention to improve patient survival. Here, we confirmed that the NEPC cell line H660 is devoid of the commonly targeted prostate biomarkers AR, PSMA, and prostate-specific antigen but selectively expresses DLL3 on the cell surface. However, this is an idealized preclinical model, and a varied range of prostate biomarker expression may still be observed in patients with NEPC lesions. In our previous work using the SCLC tumor model H82, we successfully showed that, though expression of DLL3 is less abundant than other commonly imaged tumor-associated antigens (e.g., human epidermal growth factor receptor 2, human epidermal growth factor receptor, and PSMA), the highly tumor-restricted cell surface expression of DLL3 on SCLC allows for successful PET imaging (10). Although the expression levels of DLL3 observed in the H660 NEPC tumor cells were lower than in the H82 SCLC tumor cells, PET imaging was still feasible because of the absence of detectable cell surface DLL3 in nonmalignant cells. We demonstrated that ⁸⁹Zr-DFO-SC16 shows high specific uptake in H660 (DLL3-positive) tumors through biodistribution studies and PET imaging. PET imaging in a dual tumor model with H660 (DLL3-positive/PSMA-negative) and LNCaP (DLL3-negative/PSMA-positive) tumor cells demonstrated an inability to detect PSMA-negative NEPC lesions with other commonly used imaging approaches. Neuroendocrine differentiation in prostate adenocarcinoma lesions due to selective treatment pressure can lead to the activation of different pathways, including the possibility of low AR and low AR-pathway signaling, which may result in the inability to detect such lesions with ⁶⁸Ga-PSMA-11 (14)

or other AR-targeted tracers such as ¹⁸F-16 β -fluoro-5 α -dihydrotestosterone (12,21). Therefore, using ⁶⁸Ga-PSMA-11 only, NEPC lesions may not be detected.

DLL3 imaging can provide patient stratification and suggests a rationale for DLL3-targeted therapeutic approaches. Four DLL3-specific therapies have been tested clinically: the antibody–drug conjugate rovalpituzumab tesirine, the bispecific T cell engager AMG757, the chimeric antigen receptor T cell AMG119, and the trispecific T-cell engager HPN328. Rovalpituzumab tesirine therapy demonstrated minimal responses in SCLC and other neuroendocrine carcinomas (9/69; 13%) (22), whereas AMG757 (NCT03319940), AMG119 (NCT03392064), and HPN328 (NCT04471727) are currently being tested in SCLC patients in first-in-humans studies. One avenue yet to be explored could use a targeted radionuclide therapy with ¹⁷⁷Lu in patients with detected DLL3-positive PC lesions via ⁸⁹Zr-DFO-SC16 PET. Recent work by our lab has demonstrated the

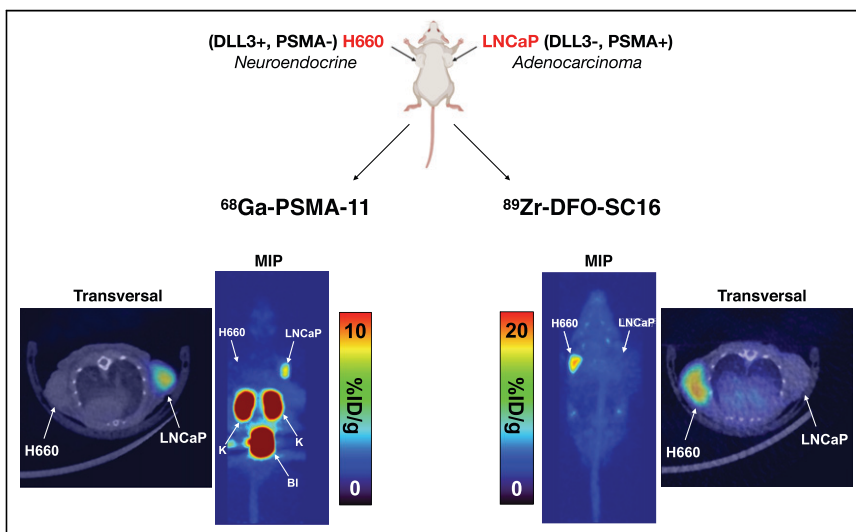


FIGURE 5. ⁶⁸Ga-PSMA-11 cannot image NEPC lesions in vivo. Shown are PET images of ⁶⁸Ga-PSMA-11 (1 h after injection) or ⁸⁹Zr-DFO-SC16 (120 h after injection) in male athymic nude mouse bearing H660 and LNCaP tumors xenografted on left and right shoulders, respectively. MIP = maximum-intensity projection.

exceptional efficacy of ^{177}Lu -labeled-SC16 for the treatment of SCLC in preclinical models (23).

Lastly, we demonstrated an inability to target SSTRs in a subcutaneous NEPC model. Reports on the presence of SSTRs in NEPC have been contradictory and inconclusive, with some studies suggesting that SSTR2 expression is upregulated (24,25) whereas others have shown low or absent expression (26,27). Here, we showed that H660 tumor cells do not express SSTRs and therefore cannot be imaged *in vivo* through somatostatin-based receptor PET imaging.

Although DLL3 appears to be a potential target for PET imaging in NEPC lesions, the biologic consequences of PC treatments on preexisting NEPC lesions are not understood. PC lesions in patients may have distinct adenocarcinoma, neuroendocrine, or mixed phenotypes. Therefore, even with detection of NEPC, patients may continue ADT. ADT influences the expression of prostate-specific antigen and PSMA and blocks AR-targeting agents and therefore influences the outcomes of PET imaging studies that are specific for these targets (28–30). There is no clear understanding of the biologic consequence of ADT on neuroendocrine cells or on the expression of DLL3. Likewise, it has been shown that the phosphatidylinositol 3-kinase pathway is activated in ADT-resistant mCRPC and influences the expression of neuroendocrine markers (31,32). Two phosphatidylinositol 3-kinase inhibitors, everolimus (NCT00976755) and BKM-120 (NCT01385293), are in clinical trials for mCRPC. Further studies to evaluate the potential influence of PC treatments on NEPC lesions and DLL3 expression are warranted.

Overall, the selective expression of DLL3 in the tumor, with no detectable expression in nonmalignant cells, and the high specificity of tumor uptake of ^{89}Zr -DFO-SC16 suggest the possibility of translating this imaging method into the clinic. With a clinical trial (NCT04199741) currently under way at Memorial Sloan Kettering Cancer Center—the first-in-humans clinical trial of DLL3 PET imaging in patients with SCLC—our data encourage the use of DLL3 PET imaging in patients with NEPC lesions. Ultimately, DLL3-targeted PET imaging might confirm the presence of NEPC lesions through a noninvasive whole-body PET scan, aid patient selection, and improve therapeutic outcomes in NEPC-directed clinical trials.

CONCLUSION

These findings suggest that ^{89}Zr -DFO-SC16 is a noninvasive diagnostic PET agent that can be used as a tool to detect the presence of DLL3-positive NEPC lesions at single-lesion resolution. We hope these findings will improve on the current approach of biopsy-based and genotypic characterization in identifying these patients.

DISCLOSURE

The study was supported in part by NIH T32 GM073546 (Joshua Korsen), NIH R35 CA232130-01A1 (Jason Lewis), R35 CA263816 (Charles Rudin), the Geoffrey Beene Cancer Research Center (Jason Lewis, Nagavarakishore Pillarsetty, Charles Rudin, and Yu Chen), and the Department of Defense Idea Award grant W81XWH-19-1-0536 (Nagavarakishore Pillarsetty). The Radiochemistry and Molecular Imaging Probes Core Facility, the Small Animal Imaging Facility, and the Molecular Cytology Core Facility were supported in part by NIH P30 CA08748. Goutam Chakraborty is supported by a Prostate Cancer Foundation Young Investigator Award. Jason Lewis is an associate editor of *The*

Journal of Nuclear Medicine but had no involvement or access to information regarding the peer review of this article. No other potential conflict of interest relevant to this article was reported.

ACKNOWLEDGMENTS

We acknowledge the Radiochemistry and Molecular Imaging Probes Core Facility, the Small Animal Imaging Facility, and the Molecular Cytology Core Facility. The graphical abstract and part of Figure 5 were made in Biorender.com.

KEY POINTS

QUESTION: Can DLL3-targeted PET be used as a tool for the noninvasive diagnosis of NEPC?

PERTINENT FINDINGS: DLL3 is expressed exclusively on the cell surface of the H660 NEPC cell line and can be detected with the DLL3-targeting tracer ^{89}Zr -DFO-SC16. *In vivo* PET imaging studies showed that ^{89}Zr -DFO-SC16 is selective for DLL3-expressing NEPC lesions and cannot be imaged with ^{68}Ga -PSMA-11 or ^{68}Ga -DOTATATE. The selective expression of DLL3 in the tumor and specific tumor uptake of ^{89}Zr -DFO-SC16 suggest potential translation of this imaging method to the clinic.

IMPLICATIONS FOR PATIENT CARE: PET imaging of DLL3 may allow for the identification of NEPC in patients in a benign, noninvasive way early enough to better inform clinical decision making.

REFERENCES

1. Watson PA, Arora VK, Sawyers CL. Emerging mechanisms of resistance to androgen receptor inhibitors in prostate cancer. *Nat Rev Cancer*. 2015;15:701–711.
2. Bluemn EG, Coleman IM, Lucas JM, et al. Androgen receptor pathway-independent prostate cancer is sustained through FGF signaling. *Cancer Cell*. 2017;32:474–489.e6.
3. Quintanal-Villalonga Á, Chan JM, Yu HA, et al. Lineage plasticity in cancer: a shared pathway of therapeutic resistance. *Nat Rev Clin Oncol*. 2020;17:360–371.
4. Davies AH, Beltran H, Zoubeidi A. Cellular plasticity and the neuroendocrine phenotype in prostate cancer. *Nat Rev Urol*. 2018;15:271–286.
5. Ku SY, Rosario S, Wang Y, et al. Rb1 and Trp53 cooperate to suppress prostate cancer lineage plasticity, metastasis, and antiandrogen resistance. *Science*. 2017;355:78–83.
6. Borromeo MD, Savage TK, Kollipara RK, et al. ASCL1 and NEUROD1 reveal heterogeneity in pulmonary neuroendocrine tumors and regulate distinct genetic programs. *Cell Rep*. 2016;16:1259–1272.
7. Owen DH, Giffin MJ, Bailis JM, Smit MD, Carbone DP, He K. DLL3: an emerging target in small cell lung cancer. *J Hematol Oncol*. 2019;12:61.
8. Puca L, Gavryert K, Sailer V, et al. Delta-like protein 3 expression and therapeutic targeting in neuroendocrine prostate cancer. *Sci Transl Med*. 2019;11:eaav0891.
9. Saunders LR, Bankovich AJ, Anderson WC, et al. A DLL3-targeted antibody-drug conjugate eradicates high-grade pulmonary neuroendocrine tumor-initiating cells *in vivo*. *Sci Transl Med*. 2015;7:302ra136.
10. Sharma SK, Pourat J, Abdel-Atti D, et al. Noninvasive interrogation of DLL3 expression in metastatic small cell lung cancer. *Cancer Res*. 2017;77:3931–3941.
11. Beltran H, Hruszkewycz A, Scher HI, et al. The role of lineage plasticity in prostate cancer therapy resistance. *Clin Cancer Res*. 2019;25:6916–6924.
12. Fox JJ, Gavane SC, Blanc-Autran E, et al. Positron emission tomography/computed tomography-based assessments of androgen receptor expression and glycolytic activity as a prognostic biomarker for metastatic castration-resistant prostate cancer. *JAMA Oncol*. 2018;4:217–224.
13. Schwarzenboeck SM, Rauscher I, Bluemel C, et al. PSMA ligands for PET imaging of prostate cancer. *J Nucl Med*. 2017;58:1545–1552.
14. Bakht MK, Derecichei I, Li Y, et al. Neuroendocrine differentiation of prostate cancer leads to PSMA suppression. *Endocr Relat Cancer*. 2018;26:131–146.
15. Holland JP, Sheh Y, Lewis JS. Standardized methods for the production of high specific-activity zirconium-89. *Nucl Med Biol*. 2009;36:729–739.

16. Sharma SK, Lyashchenko SK, Park HA, et al. A rapid bead-based radioligand binding assay for the determination of target-binding fraction and quality control of radiopharmaceuticals. *Nucl Med Biol.* 2019;71:32–38.
17. Mu P, Zhang Z, Benelli M, et al. SOX2 promotes lineage plasticity and anti-androgen resistance in TP53- and RB1-deficient prostate cancer. *Science.* 2017; 355:84–88.
18. You S, Knudsen BS, Erho N, et al. Integrated classification of prostate cancer reveals a novel luminal subtype with poor outcome. *Cancer Res.* 2016;76:4948–4958.
19. Ross-Adams H, Lamb AD, Dunning MJ, et al. Integration of copy number and transcriptomics provides risk stratification in prostate cancer: a discovery and validation cohort study. *EBioMedicine.* 2015;2:1133–1144.
20. Luboldt W, Zophel K, Wunderlich G, Abramyuk A, Luboldt HJ, Kotzerke J. Visualization of somatostatin receptors in prostate cancer and its bone metastases with Ga-68-DOTATOC PET/CT. *Mol Imaging Biol.* 2010;12:78–84.
21. Vargas HA, Kramer GM, Scott AM, et al. Reproducibility and repeatability of semi-quantitative ¹⁸F-fluorodihydrotestosterone uptake metrics in castration-resistant prostate cancer metastases: a prospective multicenter study. *J Nucl Med.* 2018;59:1516–1523.
22. Mansfield AS, Hong DS, Hann CL, et al. A phase I/II study of rovalpituzumab tesirine in delta-like 3-expressing advanced solid tumors. *NPJ Precis Oncol.* 2021;5:74.
23. Tully KM, Tendler S, Carter LM, et al. Radioimmunotherapy targeting delta-like ligand 3 in small cell lung cancer. *Clin Cancer Res.* 2022;28:1391–1401.
24. Hansson J, Bjartell A, Gadaleanu V, Dizeyi N, Abrahamsson PA. Expression of somatostatin receptor subtypes 2 and 4 in human benign prostatic hyperplasia and prostatic cancer. *Prostate.* 2002;53:50–59.
25. Morichetti D, Mazzucchelli R, Stramazzotti D, et al. Immunohistochemical expression of somatostatin receptor subtypes in prostate tissue from cystoprostatectomies with incidental prostate cancer. *BJU Int.* 2010;106:1072–1080.
26. Cariaga-Martinez AE, Lorenzati MA, Riera MA, et al. Tumoral prostate shows different expression pattern of somatostatin receptor 2 (SSTR2) and phosphotyrosine phosphatase SHP-1 (PTPN6) according to tumor progression. *Adv Urol.* 2009; 2009:723831.
27. Hennigs JK, Muller J, Adam M, et al. Loss of somatostatin receptor subtype 2 in prostate cancer is linked to an aggressive cancer phenotype, high tumor cell proliferation and predicts early metastatic and biochemical relapse. *PLoS One.* 2014;9: e100469.
28. Blee AM, Huang H. Lineage plasticity-mediated therapy resistance in prostate cancer. *Asian J Androl.* 2019;21:241–248.
29. Sasaki T, Sugimura Y. The importance of time to prostate-specific antigen (PSA) nadir after primary androgen deprivation therapy in hormone-naive prostate cancer patients. *J Clin Med.* 2018;7:565.
30. Afshar-Oromieh A, Debus N, Uhrig M, et al. Impact of long-term androgen deprivation therapy on PSMA ligand PET/CT in patients with castration-sensitive prostate cancer. *Eur J Nucl Med Mol Imaging.* 2018;45:2045–2054.
31. Crumbaker M, Khoja L, Joshua AM. AR signaling and the PI3K pathway in prostate cancer. *Cancers (Basel).* 2017;9:34.
32. Chen R, Li Y, Buttyan R, Dong X. Implications of PI3K/AKT inhibition on REST protein stability and neuroendocrine phenotype acquisition in prostate cancer cells. *Oncotarget.* 2017;8:84863–84876.